Energy Materials

Article

Achieving fast and stable Li+ transport in lithium-sulfur battery via a high ionic conduction and high adhesion solid polymer electrolyte

Ximing Cui, Xiaohui Wang, Qinmin Pan[*]

School of Chemistry and Chemical Engineering, Harbin Institute of Technology, Harbin 150001, Heilongjiang, China.

***Correspondence to:** Prof. Qinmin Pan, School of Chemistry and Chemical Engineering, Harbin Institute of Technology, No. 92, Xidazhi Street, Nangang District, Harbin 150001, Heilongjiang, China. E-mail: panqm@hit.edu.cn

Abstract

Solid-state lithium (Li)-sulfur (S) batteries are promising secondary batteries because of their high energy density and high safety, but their practical application is severely hindered by poor Li-ions (Li+) transport in batteries due to low ionic conduction of the electrolyte and unstable electrode/electrolyte interface. Here, we address the issue by using a polyurethane (PU)-based electrolyte. The polar urethane/urea groups of PU reduce the hopping energy barrier of Li+, which results in high ionic conductivity of 1.8×10^{-4} S cm^{-1} (25 °C), high ion transference number of 0.54, and low activation energy of 0.39 eV. In addition, the polar urethane/urea groups endow the electrolyte with high adhesion, which allows the electrode/electrolyte interfaces to self-heal timely after being damaged during cycling. Benefiting from these merits, a symmetric Li||Li cell using the polyolefin-PU-bis(trifluoromethane)sulfonimide lithium salt electrolyte can cycle for approximately 800 h with a stable overpotential (approximately 40 mV), and a solid-state Li-S battery using the electrolyte delivers a specific capacity of approximately 610 mAh g^{-1} after testing for 125 cycles at a S loading of about 4 mg cm^{-2}. Self-healing of the electrode/electrolyte interfaces during cycling was observed *in situ* by a laser confocal microscope. This study demonstrates the importance of polar groups in electrolytes in maintaining a fast and stable Li+ transport, which can be applied to other solid-state batteries.

Keywords: Solid-state Li-S battery, urethane/urea groups, low energy barrier, self-healing electrode/electrolyte interface, *in-situ* observation

INTRODUCTION

Solid-state lithium (Li)-sulfur (S) batteries are considered to be the most promising secondary batteries because of their high energy density (2,550 Wh kg^{-1}) and high safety[1-8]. However, solid-state Li-S batteries often suffer from poor Li-ions (Li$^+$) transport in batteries due to low ionic conduction of the electrolyte and unstable electrode/electrolyte interface during the charge/discharge processes [Figure 1A][9-15]. The poor Li$^+$ transport severely hinders the practical application of solid-state Li-S batteries[16-20].

Recently, many groups have designed electrolytes with high ionic conductivity and high mechanical strength to improve the ionic conduction of electrolytes and the stability of the electrode/electrolyte interface[1-8]. These electrolytes include ceramic electrolytes and solid polymer electrolytes (SPE). Although ceramic electrolytes generally exhibit high ionic conductivity and high strength, they often show poor contact with electrodes, which affects the Li$^+$ transport in the electrode/electrolyte interface[1,6]. In contrast, flexible polymer electrolytes can well contact with electrodes, but they exhibit relatively low room-temperature ionic conductivity and low mechanical strength[9-12]. A common method to improve the ionic conductivity of polymer electrolytes is to introduce plasticizers (such as Pyr$_{13}$FSI, hydroxypropyl trimethylammonium bis (trifluoromethane) sulfonimide chitosan salt (HACC-TFSI), *etc.*) or nanofillers (such as Ai$_2$O$_3$, TiO$_2$-TiN, Li$_7$La$_3$Zr$_2$O$_{12}$, *etc.*)[11,13-17]. The plasticizers and nanofillers reduce the crystallinity of the polymer electrolytes, thus resulting in high ionic conductivity[14-17]. An alternative way to realize high ionic conductivity is to prepare polymer-in-salt electrolytes (the content of lithium salt exceeding 50 wt%) [8-20]. For polymer-in-salt electrolytes, Li$^+$ can transport in their amorphous polymer regions through the movement of polymer segments and through the ionic channels constructed by aggregated cation/anion clusters[18].

SPE usually composite inorganic materials to improve their mechanical strength[6,21,22]. The composite polymer electrolytes (such as polyethylene oxide (PEO)/Li$_{1.3}$Al$_{0.3}$Ti$_{1.7}$(PO$_4$)$_3$/bis(trifluoromethane)sulfonimide lithium salt (LiTFSI), PEO/Li$_7$La$_{2.75}$Ca$_{0.25}$Zr$_{1.75}$Nb$_{0.25}$O$_{12}$/LiTFSI, PEO/polyvinylidene difluoride (PVDF)/boron-nitride/LiTFSI, *etc.*) combine good flexibility of the polymer components and high strength of the inorganic components. The high strength can inhibit the growth of lithium dendrites, resulting in a stable electrode/electrolyte interface. The above studies solved the Li$^+$ transport problems of solid-state Li-S batteries to a certain extent, but it is still difficult for solid-state batteries to maintain fast and stable Li$^+$ transport during long-term cycles.

Herein, we demonstrate that fast and stable Li$^+$ transport can be achieved using a polyurethane (PU)-based electrolyte (polyolefin (PO)-PU-LiTFSI) with high ionic conduction and high adhesion. The polar urethane/urea groups of the electrolyte reduce the hopping energy barrier of Li$^+$, which contribute to high ionic conductivity (1.8 × 10^{-4} S cm^{-1}), high ion transference number (0.54), and low activation energy (0.39 eV), thereby achieving fast Li$^+$ transport. At the same time, the polar urethane/urea groups of PU endow the electrolyte with high adhesion, ensuring tight interfacial contact and self-healing electrode/electrolyte interface [Figure 1B], leading to stable Li$^+$ transport. Benefiting from the fast and stable Li$^+$ transport, a symmetric Li||Li cell using the PO-PU-LiTFSI electrolyte exhibits excellent cycling stability up to 800 h and a low overpotential of approximately 40 mV. A solid-state Li-S battery using the electrolyte displays a specific capacity of approximately 610 mAh g^{-1} even after testing for 125 cycles (S loading = 4 mg cm^{-2}). The robust electrode/electrolyte interface during cycling was observed *in situ* using a laser confocal microscope. Our study demonstrates the importance of polar groups in electrolytes in maintaining fast and stable Li$^+$ transport. This concept can also be used to solve similar problems of other solid-state batteries.
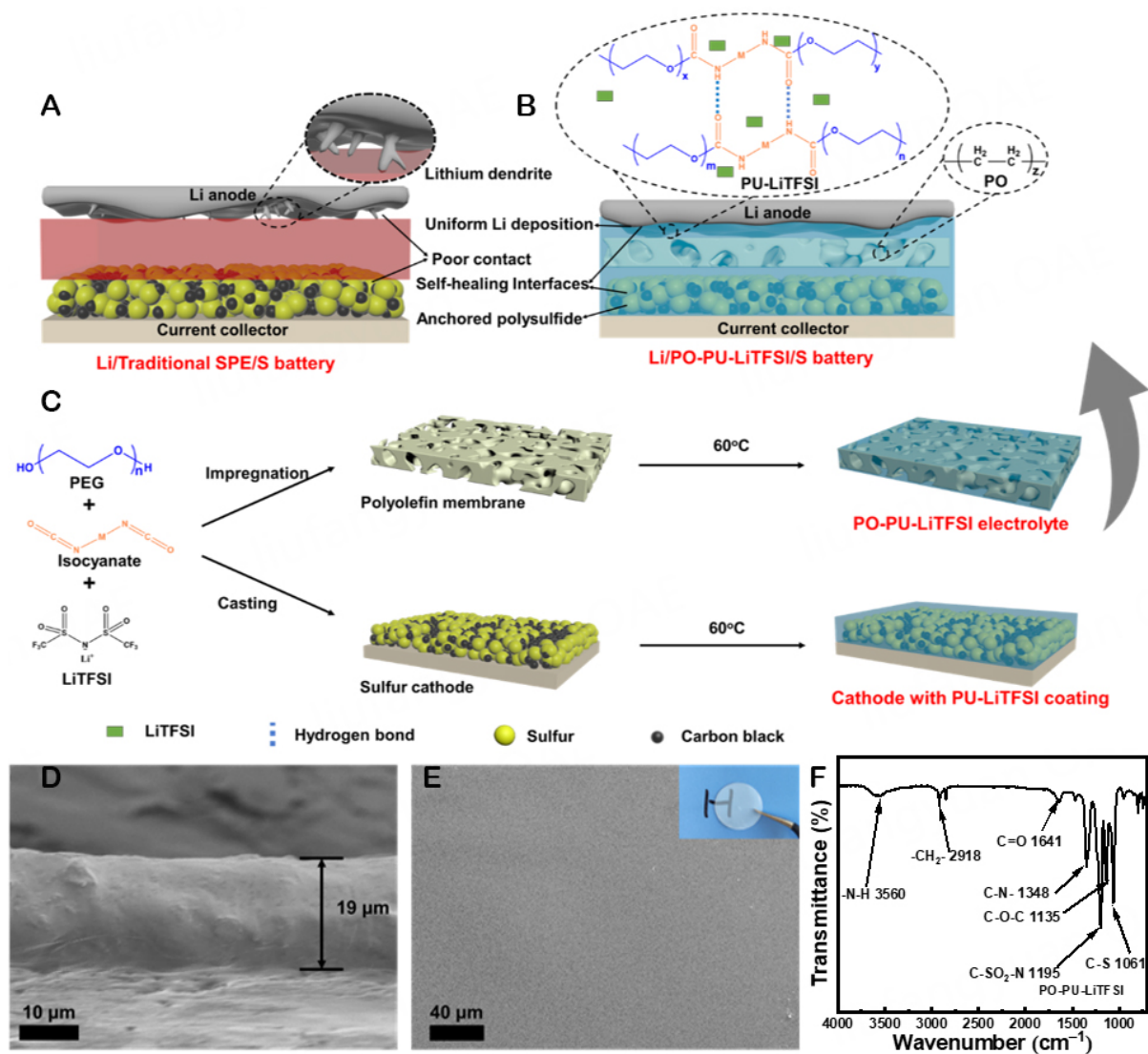
Figure 1. Schematic illustrations of solid-state Li-S batteries using (A) traditional solid polymer electrolyte (SPE) and (B) the PO-PU-LiTFSI electrolyte, (C) fabrication of the PO-PU-LiTFSI electrolyte and sulfur cathode. SEM images from (D) cross-sectional and (E) top view of the PO-PU-LiTFSI electrolyte, the inset is an optical image of the electrolyte. (F) FTIR spectrum of the PO-PU-LiTFSI electrolyte.

RESULTS AND DISCUSSION

The synthesis of the PO-PU-LiTFSI electrolyte is given in Figure 1C. First, polyethylene glycol (PEG) and isocyanate were dissolved in acetonitrile. After stirring at 60 °C for several hours, LiTFSI was added to the above solution, and the resulting mixture was coated on the PO membrane. The obtained membrane was heated in an oven at 60 °C to remove the acetonitrile. After removing the solvent, the PO-PU-LiTFSI electrolyte was obtained. The obtained electrolyte has a uniform thickness (about 19 μm) and a smooth surface [Figure 1D and E].

To identify the composition of the PO-PU-LITFSI electrolyte, Fourier transform infrared (FTIR) spectra and thermogravimetric analysis (TGA) curves were recorded. As shown in Figure 1F, the existence of -N-H bonds (3,560 cm^{-1}), C-N- bonds (1,348 cm^{-1}), and C=O bonds (1,641 cm^{-1}) indicates the existence of urethane/urea groups formed by polyaddition. No peak of isocyanate (-NCO) stretching band is found at

approximately 2,300 cm^{-1}, which indicates that isocyanate has been completely consumed by the polyaddition reaction. The existence of C-SO$_2$-N bonds (1,195 cm^{-1}) and C-S bonds (1,061 cm^{-1}) is associated with LiTFSI. The existence of the -CH$_2$- component (2,918 cm^{-1}) and C-O-C bonds (1,135 cm^{-1}) is assigned to PU segments. We also recorded FTIR spectra of the PO membrane and PU-LITFSI (PO-PU-LITFSI electrolyte without PO membrane). After adding the PO skeleton to PU-LiTFSI, the peak positions of PU-LiTFSI did not shift and no additional peaks were observed, indicating that the PO skeleton does not react with other components and exists stably in the PO-PU-LiTFSI electrolyte [Supplementary Figure 1]. Furthermore, TGA reveals that the PO and PU contents were 5 wt% and 15 wt%, respectively [Supplementary Figure 2][23].

The PO-PU-LiTFSI electrolyte shows high mechanical strength. As shown in Figure 2 A and Supplementary Figure 3, the puncture resistance of the PO-PU-LiTFSI electrolyte is as high as 4.6 N, and its tensile strength is 145.1 MPa. The tensile strength of the PO-PU-LiTFSI electrolyte is one of the best performances among reported SPE [Supplementary Table 1]. The high strength of the electrolyte is related to the high strength of the PO membrane. The puncture resistance and tensile strength of the PO-PU-LiTFSI electrolyte are about 10% higher than those of the PO membrane, which indicates that PU-LiTFSI modification can improve the strength of the PO skeleton.

The PO-PU-LiTFSI electrolyte exhibits high adhesion. The adhesive force between the PO-PU-LiTFSI electrolyte and S cathode is 4.15 N, and the value between the electrolyte and Li anode is 2.36 N [Figure 2B and Supplementary Figure 4A]. The high adhesion is related to high mobility of PU segments and the strong interactions (such as H-bonding) between urethane/urea groups and other polar groups[24]. The high mobility of PU segments was reflected by the differential scanning calorimetry (DSC) curves and X-ray diffraction (XRD) patterns. As shown in the DSC curves [Figure 2C], the peak at approximately -35 °C corresponds to the glass transition temperature (T_g) of the amorphous PU segments and the peak at approximately 45 °C corresponds to the melting point (T_m) of the crystalline PU segments[23]. The DSC curve of the PU-LiTFSI (LiTFSI: 80 wt%) shows no obvious peak at approximately 45 °C, indicating that the PU segments in the electrolyte are amorphous. Meanwhile, no sharp diffraction peaks are detected at the XRD pattern [Supplementary Figure 5], which also indicates the low crystallinity of PU segments.

The high mobility of PU segments is associated with the plasticizing effect of dissociated LiTFSI in the PO-PU-LiTFSI electrolyte [Figure 3A]. The plasticizing effect enhances with increasing LiTFSI content [Supplementary Figure 4B]. In contrast, LiTFSI in the PO-PEO-LiTFSI electrolyte cannot be dissociated at a high content. Therefore, the PEO segments in the PO-PEO-LiTFSI electrolyte exhibit poor mobility, resulting in poor contact with electrode [Figure 2B and C, Supplementary Figures 4A and 6]. The high LiTFSI dissociation in the PO-PU-LiTFSI electrolyte is related to a strong interaction between urethane/urea groups and TFSI$^-$. Density functional theory (DFT) calculations indicate that the binding energies (E_{ads}) between the urethane/urea group and TFSI$^-$ are 0.76 eV, respectively, which is higher than the values between ether oxygen of PEO and TFSI$^-$ [Figure 3B]. The high binding energy can promote the dissociation of LiTFSI[25,26]. The interaction between urethane/urea groups and TFSI$^-$ was also reflected by the FTIR spectra of PU and PU-LiTFSI [Supplementary Figure 6]. After adding LiTFSI to PU, the N-H peak of PU shifted from 3,543 to 3,560 cm^{-1}, while the C-N peak shifted from 1,360 to 1,348 cm^{-1}. In addition, the C-O-C peak shifted from 1,107 to 1,135 cm^{-1}. These peak shifts indicated the interaction between urethane/urea groups and TFSI$^-$.

The PO-PU-LiTFSI electrolyte exhibits high ionic conduction. The room-temperature ionic conductivity ($\sigma = 1.8 \times 10^{-4}$ S cm^{-1}), Li$^+$ transference number ($t_+ = 0.54$) and Li$^+$ diffusion coefficient
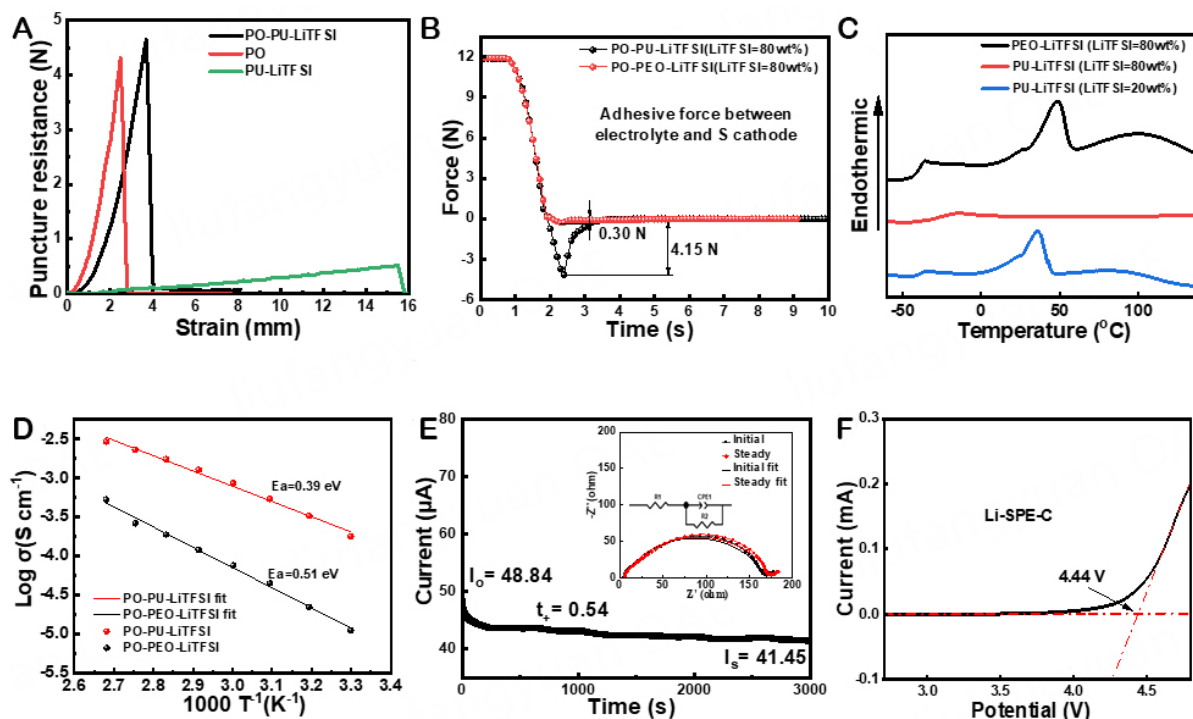
Figure 2. (A) Puncture resistance-strain curves of the electrolytes. (B) Measurements of the adhesive force between different electrolytes and sulfur cathodes. (C) DSC curves of the PEO-LiTFSI and PU-LiTFSI with different LiTFSI content. (D) Arrhenius plot of the PO-PU-LiTFSI electrolyte and PO-PEO-LiTFSI electrolyte at an increased temperature from 30 to 100 °C. (E) Chronoamperometry curve for a Li||Li symmetric cell using the PO-PU-LiTFSI electrolyte; the inset is impedance spectra before and after the polarization. (F) LSV (from the open circuit potential to 5.0 V) profile of the PO-PU-LiTFSI electrolyte at a scanning rate of 0.1 mV s^{-1}.
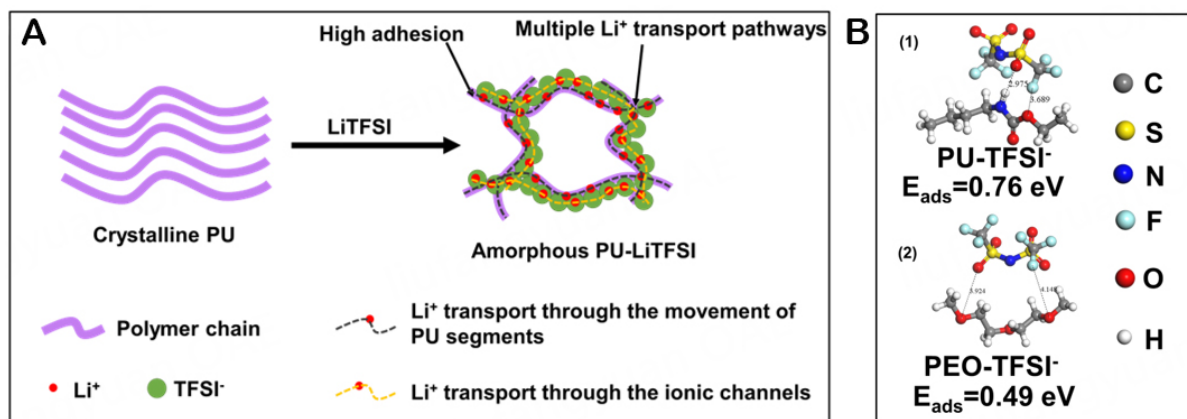

Figure 3. (A) Molecular mechanism of the high adhesion of the PO-PU-LiTFSI electrolyte and the multiple Li$^+$ transport pathways in the PO-PU-LiTFSI electrolyte. (B) DFT calculation results of the adsorption binding energy between (1) TFSI$^-$ and PU, (2) TFSI$^-$ and PEO.

($D_{Li^+} = 9.27 \times 10^{-10}$ cm^2 s^{-1}) of the PO-PU-LiTFSI electrolyte are higher than those of the PEO-based electrolyte ($\sigma = \sim5 \times 10^{-5}$ S cm^{-1}, $t_+ = \sim0.2$) [Figure 2D and E, Supplementary Figure 7][27-29].

The activation energy (E_a) based on the Arrhenius plots for the PO-PU-LiTFSI electrolyte is 0.39 eV, which is lower than those of the PEO-based electrolyte ($E_a = 0.51$ eV). High ionic conductivity, high Li$^+$ transference number, high Li$^+$ diffusion coefficient, and low activation energy are associated with polar
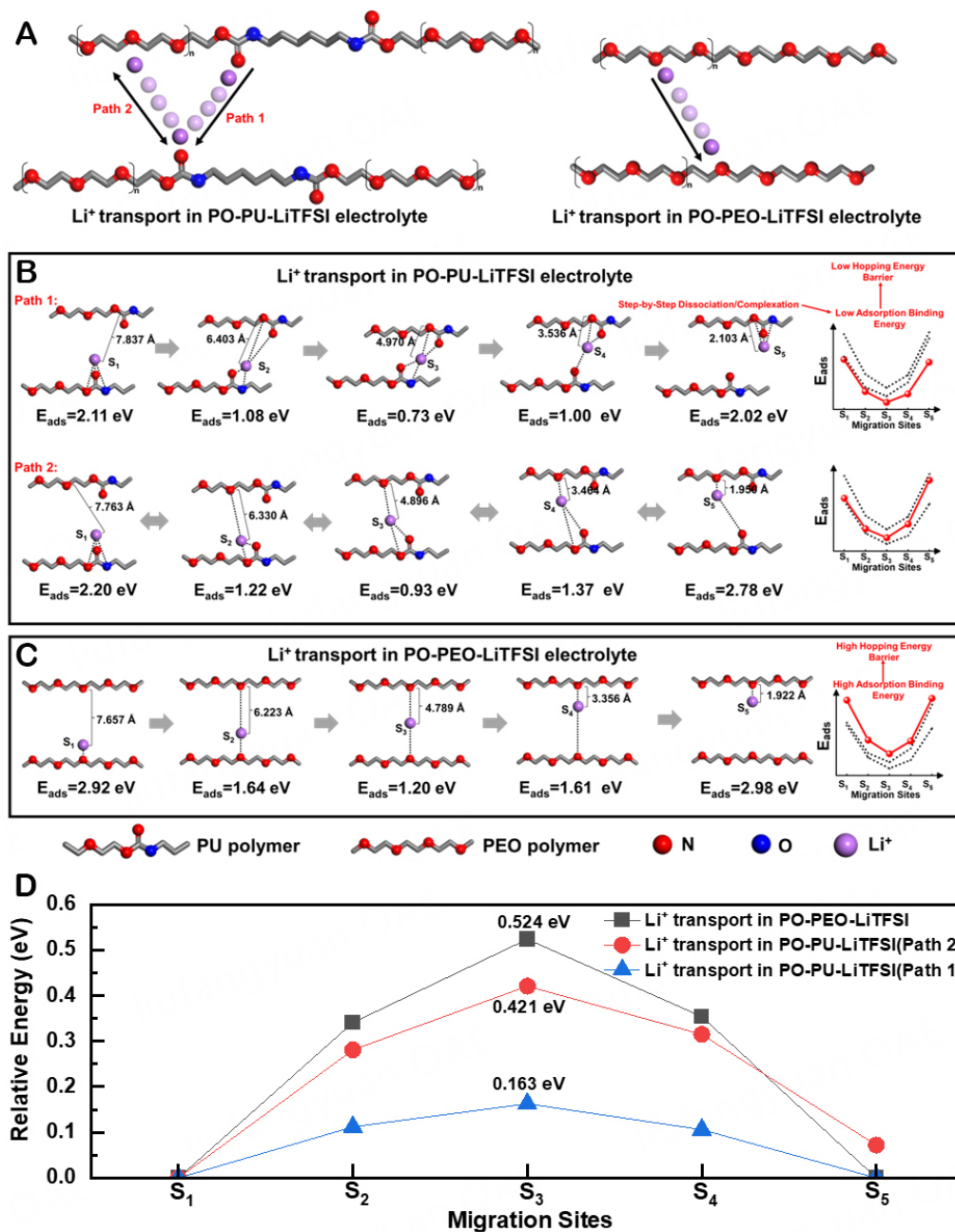
Figure 4. (A) Schematic illustrations of the Li$^+$ transport pathways in the PO-PU-LiTFSI electrolyte and PO-PEO-LiTFSI electrolyte. DFT calculation results of the adsorption binding energy between (B) Li$^+$ and PU polymer, (C) Li$^+$ and PEO polymer. (D) Energy diagrams of Li$^+$ transport in the PO-PU-LiTFSI electrolyte and PO-PEO-LiTFSI electrolyte.

urethane/urea groups in the PO-PU-LiTFSI electrolyte. When Li$^+$ moves in the PO-PU-LiTFSI electrolyte, it can dissociate from one bonded oxygen/nitrogen atom while still coordinating with the others [Figure 4A]. Step-by-step dissociation/complexation leads to low adsorption binding energy. It is calculated that the adsorption binding energy of different positions during Li$^+$ migration is less than those in PEO chains [Figure 4B and C]. Low adsorption binding energy contributes to low Li$^+$ transport resistance. It is calculated that when Li$^+$ is transferred between PEO chains, the required energy barrier is as high as 0.524 eV, while the energy barriers are 0.163 and 0.421 eV for the transfer between PU chains [Figure 4D].

In addition, there are multiple Li^+ transport pathways in the PO-PU-LiTFSI electrolyte [Figure 3A]. In the case of a high degree of LiTFSI dissociation and high LiTFSI content, Li^+ can transport not only through the movement of the PU segments in the amorphous regions but also through the ionic channels constructed by aggregated cation/anion clusters[18-20]. Meanwhile, the migration of $TFSI^-$ is limited by the aggregated ion clusters and the interaction between the urethane/urea group with $TFSI^-$. The dissociated lithium salts also act as plasticizers to increase the amorphous regions of the polymer electrolyte [Figure 2C and Supplementary Figure 5]. Therefore, the PO-PU-LiTFSI electrolyte exhibits high ionic conduction.

The PO-PU-LiTFSI electrolyte shows high electrochemical stability. The electrochemical stability window of the PO-PU-LiTFSI electrolyte is 4.57 V, which is higher than that of PEO-based SPE (about 4 V) [Figure 2F][30].

It is believed that the low electrochemical stability of PEO-based electrolytes is due to the high reactivity of their terminal hydroxyl groups[30]. In this study, the terminal hydroxyl groups of PEG were consumed by polyaddition reaction, so the PO-PU-LiTFSI electrolyte exhibits high electrochemical stability.

To further evaluate electrochemical performance of the PO-PU-LiTFSI electrolyte, symmetric Li||Li cells and solid-state Li-S batteries were assembled. As shown in [Supplementary Figure 8] the Li||Li cell using the PO-PU-LiTFSI electrolyte can cycle for about 800 h with a stable overpotential (about 40 mV). The results show that the electrode/electrolyte interfaces of the battery are stable, and the PO-PU-LiTFSI electrolyte exhibits high stability during cycling. At a high S loading of approximately 4 mg cm^{-1}, the solid-state Li-S battery using the PO-PU-LiTFSI electrolyte delivers a specific capacity of ~610 mAh g^{-1} after testing for 125 cycles, which is one of the best performances among related solid-state Li-S batteries [Figure 5A and Supplementary Table 1]. The solid-state Li-S battery using the electrolyte also exhibits a good rate capability [Figure 5B]. At a S loading of approximately 3 mg cm^{-1}, the solid-state Li-S battery delivers specific capacity values of 1,297, 994, and 822 mAh g^{-1} at rates of 0.05 C, 0.1 C, and 0.2 C, respectively. The cycling performance and rate capability of the solid-state battery deteriorate when the LiTFSI content in the electrolyte decreases, which is due to the poor contact between the electrolyte and the electrodes [Figure 5B and Supplementary Figure 9].

The solid-state Li-S batteries exhibit low interfacial impedance and stable electrode/electrolyte interfaces during cycling. Figure 5C records the voltage profiles of the batteries using PO-PU-LiTFSI electrolytes with different LiTFSI contents. The discharge curve of solid-state batteries displays two plateaus at 2.3 and 2.1 V, corresponding to two stages of lithiation of S_8, showing a similar discharge curve to liquid Li-S batteries. The discharge plateau at around 2.3 V is associated with the ring opening of crown S_8 and conversion into long-chain polysulfides (Li_2S_n; $3 \leq n \leq 8$). The second plateau, corresponding to about 2.1 V, is attributed to the further conversion of long-chain Li_2S_n to Li_2S. The battery using the electrolyte with 80 wt% LiTFSI content exhibits small polarization and more stable voltage profiles during cycling, indicating low interfacial impedance and excellent electrode/electrolyte interface stability. On the contrary, the battery using low-LiTFSI-content (20 wt%) electrolyte exhibits severe polarization and unstable voltage profiles, showing high interfacial impedance and unstable electrode/electrolyte interfaces.

Differences in interfacial impedance were also reflected by Nyquist plots of solid-state Li-S batteries. The solid-state battery using a high-LiTFSI-content electrolyte exhibits nearly coincident Nyquist plots at different cycles [Figure 5D]. The electrochemical impedance spectroscopy (EIS) fitting result shows small changes in ohmic resistance (R_o), interfacial charge transfer resistance (R_{ct}), and SEI layer resistance (R_{SEI}) during cycling [Supplementary Table 2]. The battery using a high-LiTFSI-content electrolyte shows a R_{ct} of
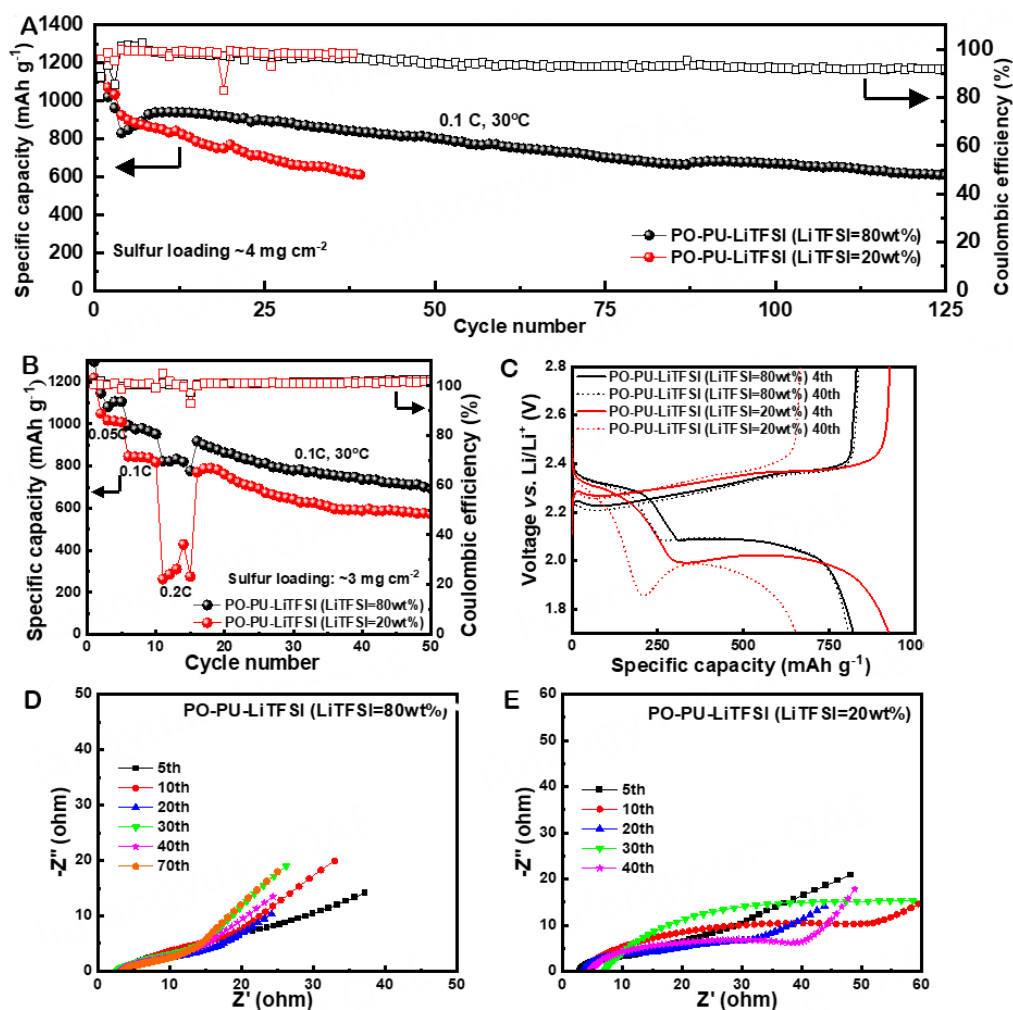
Figure 5. (A) Cycling performance, (B) rate capability, (C) charge/discharge curves, (D and E) Nyquist plots of solid-state Li-S batteries using the PO-PU-LiTFSI electrolytes with different LiTFSI contents.

approximately 6 Ω during cycling, exhibiting low interfacial impedance. In contrast, the battery using low-LiTFSI-content electrolyte exhibits unstable R_{ct} ranging from 14 to 46 Ω [Figure 5E, Supplementary Table 2].

The stable electrode/electrolyte interfaces were confirmed by SEM observation. The PO-PU-LiTFSI electrolyte (LiTFSI: 80 wt%) exhibits a uniform thickness, and no obvious cracks are observed at the electrode/electrolyte interfaces after 50th cycles [Figure 6A]. The surface of the Li anode after cycling is smooth without pores and lithium dendrites [Figure 6C]. On the contrary, there are obvious cracks between the Li anode and the low-LiTFSI-content electrolyte [Figure 6B]. The low-LiTFSI-content electrolyte is detached from the S cathode. The surface of the Li anode after cycling is covered with pores and dead Li [Figure 6D]. The stable electrode/electrolyte interfaces of the battery using high-LiTFSI-content electrolytes were also confirmed by in-situ observation through a laser confocal microscope [Figure 6E]. The shape of the electrodes changed after different charge/discharge cycles, but the electrolyte still had tight contact with the electrodes without cracks. Even if we peeled the S cathode from the electrolyte surface, the broken electrode/electrolyte interface timely recovers after a brief contact, showing the self-healing ability of the electrode/electrolyte interfaces [Figure 6F].
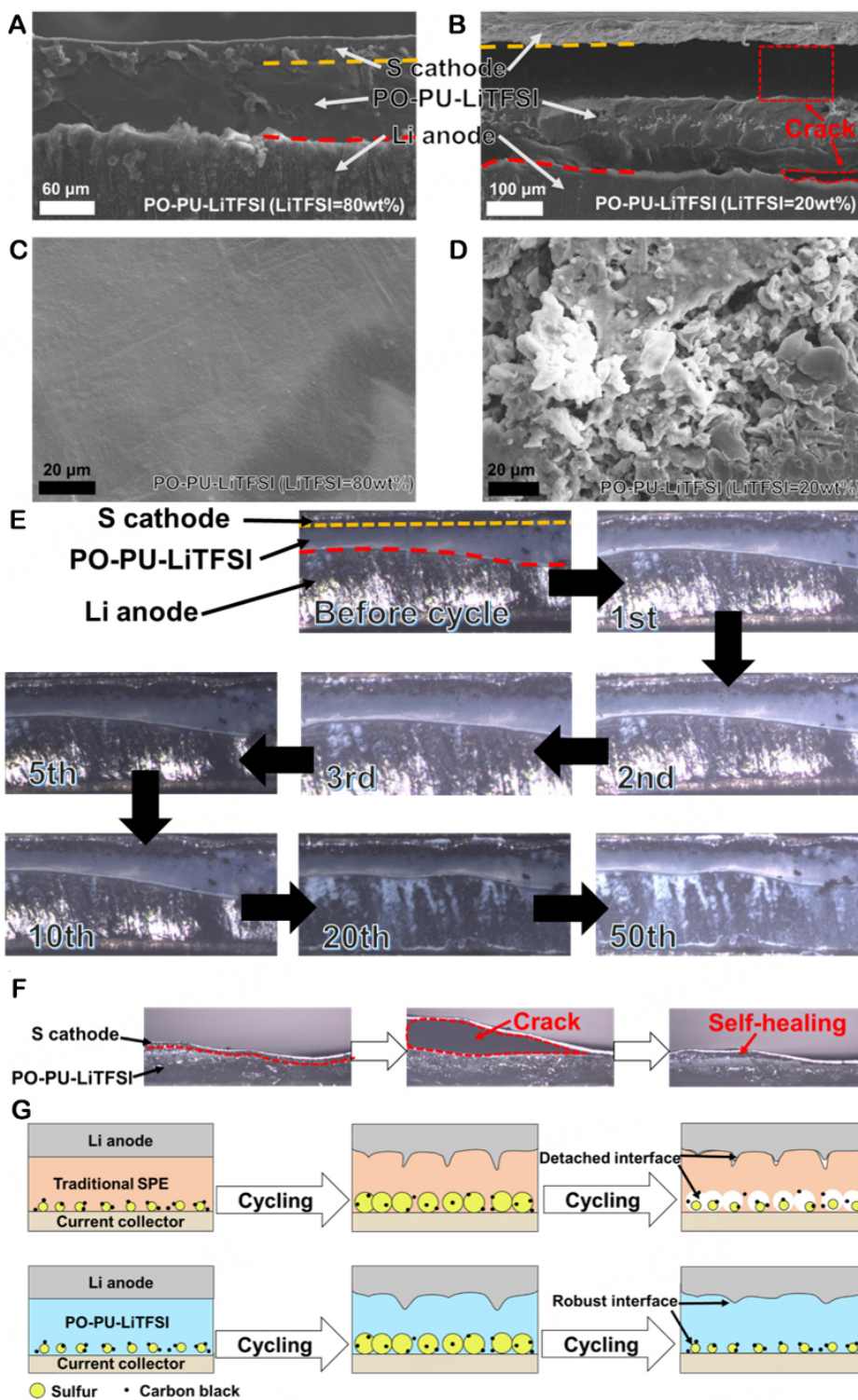
Figure 6. Cross-sectional SEM images of the solid-state Li-S batteries using the PO-PU-LiTFSI electrolytes with (A) 80 wt% and (B) 20 wt% LiTFSI content after plating/stripping for 50 cycles. SEM images of the Li anodes from the batteries using the PO-PU-LiTFSI electrolytes with (C) 80 wt% and (D) 20 wt% LiTFSI content after plating/stripping for 50 cycles. (E) *In-situ* optical microscopy images of the electrode/electrolyte interfaces of the solid-state Li-S battery after different cycles. (F) Optical microscopy images show the self-healing of the electrode/electrolyte interface. (G) Mechanism illustration of the robust interface using the PO-PU-LiTFSI electrolyte.

The excellent performance of the solid-state Li-S battery can be explained by the following factors: (1) High room-temperature ionic conductivity, high Li^+ transference number, high Li^+ diffusion coefficient, and low activation energy reduce battery internal resistance and polarization, thereby achieving fast Li^+ transport. Fast Li^+ transport is critical for the excellent electrochemical performance of Li-S batteries. (2) The high adhesion allows the electrode and electrolyte to maintain tight contact and even enables the broken electrode/electrolyte interface to self-heal during cycling, leading to stable Li^+ transport [Figure 6G]. (3) The high mechanical strength of the PO-PU-LiTFSI electrolyte inhibits the growth of lithium dendrites and prevents damage to the electrode/electrolyte interfaces [Figure 1B]. (4) For Li-S batteries, the shuttle of polysulfides between the Li anodes and S cathodes results in irreversible loss of active materials and capacity. The PO-PU-LiTFSI can prevent polysulfides from reaching the Li anode, reducing capacity loss. This effect was confirmed by DFT calculations. The binding energy between the PU segment and Li_2S_6 is 1.43 eV, which is higher than that of the PEO segment and Li_2S_6 (1.05 eV) [Supplementary Figure 10]. The Li-S batteries using the PO-PU-LiTFSI electrolyte showed much lower shuttle currents. The results suggest that the PO-PU-LiTFSI electrolyte can effectively prevent polysulfides from reaching the Li anode and thus depressing the shuttle effect. Indeed, the Li-S batteries using the PO-PU-LiTFSI electrolyte also exhibited a lower self-discharge rate at the open circuit voltage (OCV) than the Li-S batteries using the PO-PEO-LiTFSI electrolyte [Supplementary Figure 11].

A solid-state Li-S pouch cell was assembled to evaluate application prospects of the PO-PU-LiTFSI electrolyte. As shown in Figure 7A, the solid-state Li-S pouch cell delivers a specific capacity of 608 mAh g^{-1} after 100 cycles. During the subsequent 0.1 C rate, it can still cycle for 150 cycles, exhibiting a specific capacity of approximately 400 mAh g^{-1} and an average Coulombic efficiency of 99.8%. The solid-state battery also exhibits good safety. As shown in Figure 7B, a solid-state Li-S pouch cell can power light-emitting diode (LED) bulbs even after it is folded, penetrated, cut, and lit.

CONCLUSIONS

In summary, we proposed a high ionic conduction and high adhesion PO-PU-LiTFSI electrolyte for solid-state Li-S batteries with fast and stable Li^+ transport. The symmetric Li||Li cell using the PO-PU-LiTFSI electrolyte exhibited a stable overpotential of about 40 mV during cycling for 800 h. The solid-state Li-S battery using the electrolyte maintained a discharge capacity of about 610 mAh g^{-1} after 125 cycles at the S loading of about 4 mg cm^{-1}. The excellent performance was attributed to the high ionic conduction and high adhesion of the electrolyte. The high ionic conductivity ensures fast Li^+ transport in the electrolyte, while its high adhesion enables tight contact with electrodes and even enables the broken electrode/electrolyte interface to self-heal, resulting in stable electrode/electrolyte interfaces and stable Li^+ transport during cycling. The robust electrode/electrolyte interface during cycling was confirmed by in-situ observation using a laser confocal microscope. Our work demonstrates that Li^+ transport problems of solid-state Li-S batteries can be solved by using electrolytes with polar groups. This design concept has the potential to solve similar interfacial problems of other solid-state batteries.
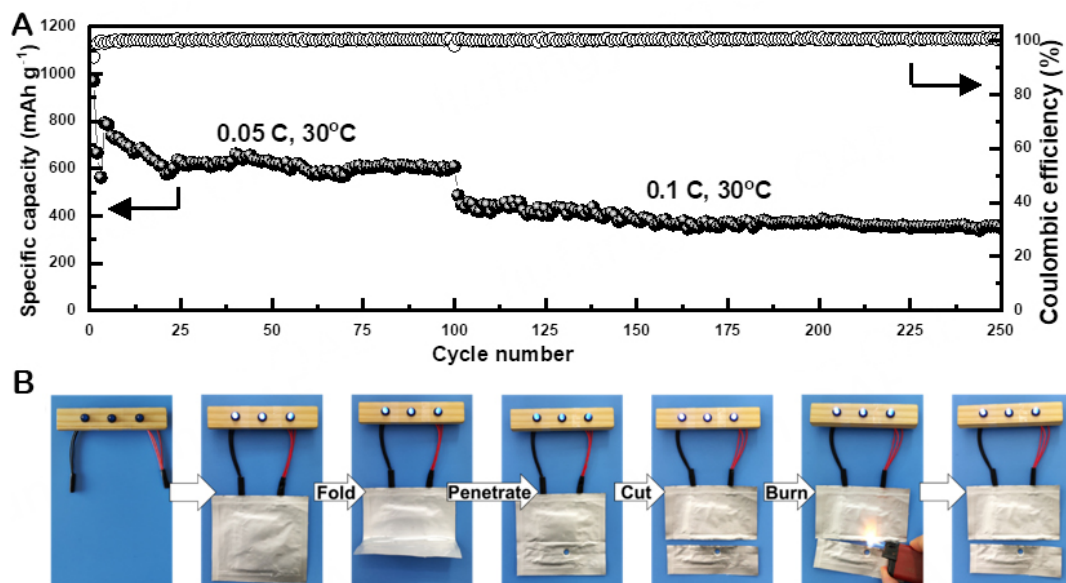
Figure 7. (A) Cycling performance of a solid-state Li-S pouch cell using the PO-PU-LiTFSI electrolyte. (B) Solid-state Li-S pouch cell using the PO-PU-LiTFSI electrolyte lighting LED bulbs under normal, folded, penetrated, cut, and burning conditions.

DECLARATIONS

Authors' contributions
Methodology, formal analysis, investigation, and writing manuscript: Cui X
Theoretical calculation: Wang X
Project administration, conceptualization, funding acquisition, and supervision: Pan Q

Availability of data and materials
The data supporting our work can be found in the Supplementary Materials.

Financial support and sponsorship
Not applicable.

Conflicts of interest
All authors declared that there are no conflicts of interest.

Ethical approval and consent to participate
Not applicable.

Consent for publication
Not applicable.

Copyright
© The Author(s) 2023.

REFERENCES

1. Yu X, Manthiram A. Electrode-electrolyte interfaces in lithium-sulfur batteries with liquid or inorganic solid electrolytes. *ACC Chem Res* 2017;50:2653-60. DOI PubMed
2. Chen R, Qu W, Guo X, Li L, Wu F. The pursuit of solid-state electrolytes for lithium batteries: from comprehensive insight to

emerging horizons. *Mater Horiz* 2016;3:487-516. DOI

3.   Wang X, Hao X, Cai D, Zhang S, Xia X, Tu J. An ultraviolet polymerized 3D gel polymer electrolyte based on multi-walled carbon nanotubes doped double polymer matrices for lithium-sulfur batteries. *Chem Eng J* 2020;382:122714. DOI

4.   Gao X, Zheng X, Tsao Y, et al. All-solid-state lithium-sulfur batteries enhanced by redox mediators. *J Am Chem Soc* 2021;143:18188-95. DOI

5.   Zhang X, Zhang T, Shao Y, et al. Composite electrolytes based on poly(ethylene oxide) and lithium borohydrides for all-solid-state lithium-sulfur batteries. *ACS Sustain Chem Eng* 2021;9:5396-404. DOI

6.   Wang Y, Wang G, He P, Hu J, Jiang J, Fan L. Sandwich structured NASICON-type electrolyte matched with sulfurized polyacrylonitrile cathode for high performance solid-state lithium-sulfur batteries. *Chem Eng J* 2020;393:124705. DOI

7.   Bag S, Zhou C, Kim PJ, Pol VG, Thangadurai V. LiF modified stable flexible PVDF-garnet hybrid electrolyte for high performance all-solid-state Li-S batteries. *Energy Stor Mater* 2020;24:198-207. DOI

8.   Wang X, Hao X, Xia Y, Liang Y, Xia X, Tu J. A polyacrylonitrile (PAN)-based double-layer multifunctional gel polymer electrolyte for lithium-sulfur batteries. *J Membr Sci* 2019;582:37-47. DOI

9.   Wang Y, Ji H, Zhang X, et al. Cyclopropenium cationic-based covalent organic polymer-enhanced poly(ethylene oxide) composite polymer electrolyte for all-solid-state Li-S battery. *ACS Appl Mater Interfaces* 2021;13:16469-77. DOI

10.   Zhu P, Yan C, Zhu J, et al. Flexible electrolyte-cathode bilayer framework with stabilized interface for room-temperature all-solid-state lithium-sulfur batteries. *Energy Stor Mater* 2019;17:220-5. DOI

11.   Sheng O, Jin C, Luo J, et al. Ionic conductivity promotion of polymer electrolyte with ionic liquid grafted oxides for all-solid-state lithium-sulfur batteries. *J Mater Chem A* 2017;5:12934-42. DOI

12.   Fang R, Xu H, Xu B, Li X, Li Y, Goodenough JB. Reaction mechanism optimization of solid-state Li-S batteries with a PEO-based electrolyte. *Adv Funct Mater* 2021;31:2001812. DOI

13.   Chen G, Bai Y, Gao Y, et al. Inhibition of crystallization of poly(ethylene oxide) by ionic liquid: insight into plasticizing mechanism and application for solid-state sodium ion batteries. *ACS Appl Mater Interfaces* 2019;11:43252-60. DOI

14.   Zeng F, Sun Y, Hui B, et al. Three-dimensional porous alginate fiber membrane reinforced PEO-based solid polymer electrolyte for safe and high-performance lithium ion batteries. *ACS Appl Mater Interfaces* 2020;12:43805-12. DOI

15.   Wang C, Wang T, Wang L, et al. Differentiated lithium salt design for multilayered PEO electrolyte enables a high-voltage solid-state lithium metal battery. *Adv Sci* 2019;6:1901036. DOI PubMed PMC

16.   Zhou T, Lv W, Li J, et al. Twinborn TiO_2-TiN heterostructures enabling smooth trapping-diffusion-conversion of polysulfides towards ultralong life lithium-sulfur batteries. *Energy Environ Sci* 2017;10:1694-703. DOI

17.   Tan J, Ao X, Dai A, et al. Polycation ionic liquid tailored PEO-based solid polymer electrolytes for high temperature lithium metal batteries. *Energy Stor Mater* 2020;33:173-80. DOI

18.   Liu W, Yi C, Li L, et al. Designing polymer-in-salt electrolyte and fully infiltrated 3D electrode for integrated solid-state lithium batteries. *Angew Chem Int Ed* 2021;133:13041-50. DOI

19.   Wu H, Gao P, Jia H, et al. A polymer-in-salt electrolyte with enhanced oxidative stability for lithium metal polymer batteries. *ACS Appl Mater Interfaces* 2021;13:31583-93. DOI

20.   Chen L, Fan L. Dendrite-free Li metal deposition in all-solid-state lithium sulfur batteries with polymer-in-salt polysiloxane electrolyte. *Energy Stor Mater* 2018;15:37-45. DOI

21.   Yin X, Wang L, Kim Y, et al. Thermal conductive 2D boron nitride for high-performance all-solid-state lithium-sulfur batteries. *Adv Sci* 2020;7:2001303. DOI PubMed PMC

22.   Fu K, Gong Y, Hitz GT, et al. Three-dimensional bilayer garnet solid electrolyte based high energy density lithium metal-sulfur batteries. *Energy Environ Sci* 2017;10:1568-75. DOI

23.   Guo Y, Qu X, Hu Z, Zhu J, Niu W, Liu X. Highly elastic and mechanically robust polymer electrolytes with high ionic conductivity and adhesiveness for high-performance lithium metal batteries. *J Mater Chem A* 2021;9:13597-607. DOI

24.   Wang Y, Gozen A, Chen L, Zhong W. Gum-like nanocomposites as conformable, conductive, and adhesive electrode matrix for energy storage devices. *Adv Energy Mater* 2017;7:1601767. DOI

25.   Lopez J, Mackanic DG, Cui Y, Bao Z. Designing polymers for advanced battery chemistries. *Nat Rev Mater* 2019;4:312-30. DOI

26.   Pan Q, Smith DM, Qi H, Wang S, Li CY. Hybrid electrolytes with controlled network structures for lithium metal batteries. *Adv Mater* 2015;27:5995-6001. DOI

27.   Li X, Zheng Y, Duan Y, Shang M, Niu J, Li CY. Designing comb-chain crosslinker-based solid polymer electrolytes for additive-free all-solid-state lithium metal batteries. *Nano Lett* 2020;20:6914-21. DOI

28.   Zhang K, Wu F, Wang X, et al. An ion-dipole-reinforced polyether electrolyte with ion-solvation cages enabling high-voltage-tolerant and ion-conductive solid-state lithium metal batteries. *Adv Funct Mater* 2022;32:2107764. DOI

29.   Cai X, Ding J, Chi Z, Wang W, Wang D, Wang G. Rearrangement of ion transport path on nano-cross-linker for all-solid-state electrolyte with high room temperature ionic conductivity. *ACS Nano* 2021;15:20489-503. DOI PubMed

30.   Yang X, Jiang M, Gao X, et al. Determining the limiting factor of the electrochemical stability window for PEO-based solid polymer electrolytes: main chain or terminal -OH group? *Energy Environ Sci* 2020;13:1318-25. DOI